

1 **Synaptic vesicle endocytosis deficits underlie GBA-linked cognitive dysfunction** 2 **in Parkinson’s disease and Dementia with Lewy bodies**

3 D J Vidyadhara^{§,1,2,3,4}, David Bäckström^{§,1,2,5}, Risha Chakraborty^{1,2}, Jiapeng Ruan⁶, Jae-Min
4 Park^{1,2,7}, Pramod K. Mistry⁷, Sreeganga. S. Chandra^{1,2,8*}

5 ¹Departments of Neurology and ²Neuroscience, Yale University, CT, USA,

6 ³Discipline of Neuroscience and ⁴Center for Neurodegenerative Disease and Therapeutics,
7 Chicago Medical School, Rosalind Franklin University of Medicine and Science, North Chicago,
8 IL, USA

9 ⁵Department of Clinical Science, Neurosciences, Umeå University, Sweden

10 ⁶Department of Internal Medicine, Yale University, CT, USA

11 ⁷Van Andel Institute, MI, USA

12 ⁸Program in Cellular Neuroscience, Neurodegeneration and Repair, Yale University, CT, USA

13 * Corresponding Author

14 *Contact Information: sreeganga.chandra@yale.edu; Ph: +1-203-785-6172

15 [§]Contributed equally

16 **Abstract:**

17 *GBA* is the major risk gene for Parkinson’s disease (PD) and Dementia with Lewy Bodies (DLB),
18 two common α -synucleinopathies with cognitive deficits. We investigated the role of mutant *GBA*
19 in cognitive decline by utilizing *Gba* (L444P) mutant, *SNCA* transgenic (tg), and *Gba-SNCA*
20 double mutant mice. Notably, *Gba* mutant mice showed early cognitive deficits but lacked PD-like
21 motor deficits or α -synuclein pathology. Conversely, *SNCA* tg mice displayed age-related motor
22 deficits, without cognitive abnormalities. *Gba-SNCA* mice exhibited both cognitive decline and
23 exacerbated motor deficits, accompanied by greater cortical phospho- α -synuclein pathology,
24 especially in layer 5 neurons. Single-nucleus RNA sequencing of the cortex uncovered synaptic
25 vesicle (SV) endocytosis defects in excitatory neurons of *Gba* mutant and *Gba-SNCA* mice, via
26 robust downregulation of genes regulating SV cycle and synapse assembly.
27 Immunohistochemistry and electron microscopy validated these findings. Our results indicate that
28 *Gba* mutations, while exacerbating pre-existing α -synuclein aggregation and PD-like motor
29 deficits, contribute to cognitive deficits through α -synuclein-independent mechanisms, involving
30 dysfunction in SV endocytosis.

31 **Keywords:**

32 *GBA*, *SNCA*, Cognitive dysfunction, Parkinson’s disease, Parkinson’s disease with dementia,
33 Dementia with Lewy bodies, Lewy body dementia, snRNA-seq, synaptic vesicle endocytosis,
34 synaptic plasticity, α -synuclein, α -synucleinopathies

35

36

37 **Introduction:**

38 *GBA* is the major risk gene for Parkinson's disease (PD) and Dementia with Lewy Bodies (DLB)¹⁻
39 ⁶, two late-onset neurodegenerative diseases, characterized by the neuronal accumulation of
40 Lewy bodies composed of α -synuclein⁷. PD is classified as a movement disorder, although
41 dementia affects around 50% of PD patients within 10 years after symptom onset⁷. DLB is a
42 dementia, in which cognitive decline is generally the first and most predominant symptom⁷.
43 Significantly, PD patients with *GBA* mutations exhibit greater and faster cognitive decline than
44 idiopathic PD^{1,7-9}. Cognitive dysfunction in both PD and DLB, which entails visuospatial, memory,
45 and executive dysfunction, is strongly correlated with neocortical Lewy pathology⁷. However, the
46 mechanisms through which *GBA* predisposes to cognitive dysfunction, as well as to developing
47 α -synucleinopathies in general, are not well understood.

48 Homozygous or biallelic mutations in *GBA* cause the lysosomal storage disorder, Gaucher
49 disease (GD)^{10,11}. Two prevalent mutations, due to founder effects, are N370S and L444P^{12,13}.
50 GD patients have a 20-fold increased risk of developing PD accompanied by exacerbated
51 cognitive decline. Heterozygous carriers of *GBA* mutation are at 5-fold increased risk for
52 developing both PD and cognitive dysfunction^{1,2,8,9,14-18}. In the case of DLB, *GBA* and *SNCA*, the
53 gene for α -synuclein, are top GWAS hits. Interestingly, *GBA* mutations confer an even higher risk
54 of developing DLB⁴⁻⁶. *GBA* encodes glucocerebrosidase 1 (GCase1), a lysosomal hydrolase
55 responsible for breaking down the bioactive lipid glucosylceramide (GlcCer) to glucose and
56 ceramide. In the absence of GCase1, GlcCer and other glycosphingolipids accumulate.
57 Interestingly, GCase1 deficiency and glycosphingolipid accumulation are also observed in post-
58 mortem brains of patients with sporadic PD and in aging brains¹⁹⁻²². Glycosphingolipid
59 accumulation correlates with a higher burden of α -synuclein or Lewy pathology in several brain
60 areas^{20,22,23}. These genetic, clinical, and epidemiological studies emphasize the importance of
61 understanding mechanisms of *GBA*-linked cognitive dysfunction.

62 The prevailing hypothesis in the field is that *GBA* mutations lead to GCase1 deficiency, which,
63 through a combination of lysosomal dysfunction and glycosphingolipid accumulation, trigger α -
64 synuclein aggregation, resulting in Lewy body formation and consequently, disease associated
65 phenotypes. We and others have shown that glycosphingolipids can directly interact with α -
66 synuclein and promote aggregation *in vitro*^{24,25}. Our long-lived mouse models of GD carrying the
67 *Gba* N370S and L444P mutations, exhibited reduced GCase1 activity and accumulation of
68 glycosphingolipids in the liver, spleen, and brain²⁶. As GD patients with the L444P mutation have
69 pronounced cognitive deficits²⁷, in this study, we conducted a thorough, longitudinal examination
70 of *Gba* L444P mice, in conjunction with the well-established *SNCA* tg PD mice that overexpress
71 mutant human α -synuclein, and their crossbreeds, i.e. *Gba*-*SNCA* mice. We found that cognitive
72 and motor deficits are dissociable by genotype, with *Gba* mutants exhibiting cognitive deficits
73 only, *SNCA* transgenics motor difficulties only, and *Gba*-*SNCA* severe motor and cognitive
74 phenotypes. Through histopathological analyses, we show that *Gba* L444P mutant mice lack Ser-
75 129-phospho- α -synuclein (pSer129 α -syn) pathology but presence of the *Gba* mutation in *Gba*-
76 *SNCA* mice significantly exacerbates this pathology, especially in deep layers of the cortex. Thus,
77 cognitive deficits related to *Gba* mutations may emerge independently of pSer129 α -syn
78 pathology. Cortical single-nucleus RNA sequencing (snRNA-seq) analyses revealed a potential

79 role for synaptic dysfunction, in particular synaptic vesicle endocytosis (SVE) deficits in excitatory
80 neurons, contributing to the cognitive decline observed in *Gba* mutant and *Gba*-SNCA mice. SVE
81 deficits are emerging as a central mechanism of PD pathogenesis, especially in rare monogenic
82 forms of PD^{28,29}. We suggest that synaptic endocytosis dysfunction also plays a role in cognitive
83 deficits of GBA-linked PD and DLB, while greater α -synuclein pathology burden contributes to
84 worsened motor deficits.

85 **Results:**

86 ***Gba* mutation leads to cognitive dysfunction and exacerbates motor deficits in SNCA tg**
87 **mice:** To determine the relative contributions of *GBA* and *SNCA* to motor and cognitive domains,
88 we performed behavioral analyses of wild-type (WT), *Gba*, SNCA tg, and *Gba*-SNCA mouse sex-
89 balanced cohorts. We conducted longitudinal evaluations of motor behavior every 3 months to
90 establish the age of onset and progression of PD-like motor deficits compared to cognitive
91 behavior deficits.

92 Four distinct, complementary assays were used to phenotype motor deficits: the balance beam,
93 grip strength, hind limb clasping, and open-field locomotion tests. In the balance beam test, mice
94 were required to walk along a narrow beam from a well-lit area to a dark, secure box²⁹. The
95 number of runs completed in a minute and the average time per run were used to assess motor
96 performance (Fig. 1A, Supp. Fig. 1A, 1D-E). *Gba* mice consistently performed well on this task,
97 comparable to WT mice, up to 12 months. In contrast, SNCA tg mice could perform this task at 3
98 months but began showing deficits at 6 months, which worsened by 12 months. Notably, *Gba*-
99 SNCA mice demonstrated exacerbated balance deficits compared to SNCA tg mice, with
100 significant deficits appearing as early as 6 months. By 9-12 months, *Gba*-SNCA mice were
101 severely affected and unable to navigate the balance beam (Fig. 1A, Supp. Fig. 1A, 1D-E). We
102 noted similar deficits in grip strength, measured as the force exerted by either all limbs or forelimbs
103 of the mouse when gripping a pull bar of a grip strength meter. WT and *Gba* mice did not show
104 deficits, while SNCA tg mice developed age-related decline in grip strength, which was
105 exacerbated in *Gba*-SNCA mice (Fig. 1B, Supp. Fig. 1B, Supp. Fig. 2F-G).

106 WT Mice, when picked up by the tail and lowered towards a surface, extend their limbs reflexively
107 in anticipation of contact. However, mice with neurological conditions display hind limb clasping.
108 We tested the mice for 30 seconds on this maneuver and quantitated the time spent clasping (Fig.
109 1C). WT and SNCA tg mice did not show hind limb clasping. *Gba* mice showed a trend towards
110 increased clasping (Fig. 1C, Supp. Fig. 2H), whereas *Gba*-SNCA mice showed a significant
111 increase across all ages, indicating a synthetic motor phenotype (Fig. 1C, Supp. Fig. 2H).

112 Open field assay was performed to evaluate overall locomotion. Distance traveled exploring an
113 open box (Fig. 1D) was comparable among all groups across ages, except for *Gba*-SNCA mice.
114 At 9 months, a significant loss in exploration/locomotion was noted in *Gba*-SNCA mice, which
115 worsened at 12 months (Fig. 1D, Supp. Fig. 2I). No genotypes showed anxiety-like behavior, as
116 evaluated by the time spent in the inner/outer circles of the open field (Supp. Fig. 1C). There was
117 no difference across the mice strains for body weight, however, *Gba*-SNCA mice stopped gaining
118 weight after 6 months (Supp. Fig. 1J). In summary, motor assessments demonstrate that *Gba*
119 mutants do not exhibit any appreciable motor deficits. Nonetheless, *Gba* mutation significantly
120 exacerbates existing age-related motor deficits in SNCA tg mice.

121 Next, we evaluated the impact of *Gba* and SNCA mutations on cognition by employing fear
122 conditioning and novel object recognition (NOR) tests. To avoid confounds due to learning, we
123 performed these on two separate sets of mice at 3 months and 12 months, prior to and after the
124 onset of motor deficits in SNCA tg mice (Fig. 1A-D). For fear conditioning, we habituated mice to

125 standard operant boxes, followed by exposure to paired neutral stimulus (a tone) and aversive
126 stimulus (an electric shock) on the training day. Cognitively normal mice associate this pairing
127 and exhibit a conditioned fear response i.e. freezing when exposed to the tone alone on the testing
128 day (24 hours later). We counted the number of freeze episodes after start of the tone and
129 observed a conditioned fear response in WT and SNCA tg mice at both 3 and 12 months (Fig.
130 1E). However, Gba and Gba-SNCA mice did not show a significant response on the testing day,
131 especially at 12 months. While this is suggestive of cognitive impairment, the results were
132 confounded by the heightened freezing response shown by Gba and Gba-SNCA mice for aversive
133 stimulus on the training day (Fig. 1E).

134 To substantiate the cognitive findings from fear conditioning, we performed a NOR test to assess
135 recognition memory. Here, mice were presented with two similar objects (familiarization session).
136 After 18-20 hours, one of the objects was replaced by a novel object. Mice spend more time with
137 the novel object when cognitively normal (Fig. 1F). Gba mice spent significantly less time with the
138 novel object at 3 months and maintained this behavior at 12 months, suggesting an early cognitive
139 impairment (Fig. 1E). As Gba mice do not have motor problems, these results reflect memory
140 impairments. Interestingly, SNCA tg mice did not show deficits in the NOR test (Fig. 1F), whereas
141 Gba-SNCA do, which was comparable to Gba mice (Fig. 1F). Thus, our cognitive behavior assays
142 suggest that the Gba mutation alone can cause cognitive impairment, with the poor cognition in
143 Gba-SNCA mice likely driven by Gba mutation.

144 **Gba mutation exacerbates cortical α -synuclein pathology of SNCA tg mice:** α -Synuclein
145 aggregates, redistributes from presynaptic termini to the soma, and is phosphorylated at Ser129
146 in Lewy body pathology. To investigate whether Gba-mediated cognitive deficits and accelerated
147 motor deficits are associated with α -synuclein pathology, we performed immunohistochemistry on
148 3- and 12-month-old mice brains, staining for α -synuclein, pSer129 α -syn, and the neuronal
149 marker NeuN. We found that Gba mice did not exhibit increased α -synuclein levels, redistribution,
150 or accumulation of pathological pSer129 α -syn in the cortex both at 3 and 12 months (Fig. 2A-C).
151 Similar observations were made in the CA1 hippocampus and by Western blotting of whole brain
152 homogenates (Supp. Fig. 2B-I). These findings suggest that the Gba mutation alone is insufficient
153 to cause widespread α -synuclein pathology.

154 In Gba-SNCA mice, where GCase1 deficiency coexists with a pre-existing α -synuclein
155 pathology²⁶, there is significantly increased cortical α -synuclein and pSer129 α -syn levels,
156 especially at 12 months of age when compared to SNCA tg (Fig. 2A-C, Supp. Fig. 2G, I). We also
157 noted increased redistribution of α -synuclein to the neuronal soma of Gba-SNCA mice as an
158 independent measure of α -synuclein pathology (Fig. 2A, arrows, enlarged inserts). Interestingly,
159 in CA1 hippocampus, the expression of α -synuclein and pSer129 α -synuclein, and the soma
160 redistribution of α -synuclein in Gba-SNCA mice were comparable to SNCA tg mice (Supp. Fig.
161 2B-F). Thus, in contrast to the cortex, Gba mutation only nominally exacerbates pSer129 α -syn
162 pathology, mostly in synaptic layer of CA1 at 12 months (Supp. Fig. 2F). This might be in part due
163 to high expression of the human SNCA tg in the hippocampus^{26,30}.

164 Next, we examined the intensity distribution of pSer129 α -syn in cortical neurons as well as cortical
165 layer specific α -synuclein and pSer129 α -syn expression, at 3 and 12 months of age (Fig. 2A, F-
166 H). Gba mice did not show pSer129 α -syn pathology. Gba-SNCA mice had a higher intensity of
167 pSer129 α -syn pathology in cortical neurons at 3 months (median value of 20 vs 0 in WT and Gba,
168 and 11 in SNCA tg mice), which further worsened at 12 months (Fig. 2F, i and ii) (median value
169 of 47 vs 1 in WT, 0.2 in Gba, and 20 in SNCA tg mice). As the percentage of neurons expressing
170 pSer129 α -syn in Gba-SNCA was comparable to SNCA tg mice (Fig. 2D), these data suggest that
171 the burden of pSer129 α -syn per neuron in Gba-SNCA mice was greater. We did not see cortical

172 neuronal loss in any of the mice (Fig. 2A, E), indicating that the observed behavioral deficits are
173 not due to gross neurodegeneration.

174 Layer-specific analysis of α -synuclein expression revealed that cortical layer 1, which is heavily
175 innervated by neurites, showed higher expression of α -synuclein compared to other layers. (Fig.
176 2G, i and ii, 3 and 12 months). Conversely, cortical layers 5 and 6a, which predominantly consist
177 of excitatory neurons, showed higher pathological pSer129 α -syn expression in SNCA tg and Gba-
178 SNCA mice (Fig. 2H, i and ii, at 3 and 12 months), which is more evident when pSer129 α -syn
179 expression was normalized to α -synuclein (Supp. Fig. 2A, i and ii, 3 and 12 months). Together,
180 these results suggest that the Gba mutation did not independently cause α -synuclein pathology
181 but worsened pre-existing α -synuclein pathology in the cortex of SNCA tg mice, preferentially in
182 layers 5 and 6a. With our behavior experiments (Fig. 1), these observations suggest that the
183 cognitive deficits in Gba mutants emerge independently of pSer129 α -syn pathology.

184 **Gba and SNCA driven cortical single nuclei gene expression changes:** To understand
185 cellular diversity and mechanisms for GBA-linked cognitive dysfunction, we performed single
186 nucleus RNA sequencing (snRNA-seq) on cortical tissue from mice of all four genotypes (n=14;
187 3-4 mice/genotype). We chose to perform this analysis on 12-month-old mice, as Gba-SNCA mice
188 show enhanced behavioral deficits and α -synuclein pathology, while lacking gross
189 neurodegeneration in the cortex, allowing us to investigate disease-relevant mechanisms.

190
191 We dissected cortices and utilized our previous mouse brain nuclei isolation protocol³¹, followed
192 by snRNA-seq on the 10X Chromium platform. We isolated 104,750 nuclei, that after cross-
193 sample alignment, and clustering exhibited a spatial UMAP grouping uncorrelated with individual
194 samples or genotype (Fig. 3A-E, Supp. Fig. 3A, B).

195 The transcriptional signatures from 104,750 nuclei, segregated into 13 broad cortical cell type
196 clusters (Fig. 3D, E), exhibiting specific expressions of established cell-type markers (Supp. Fig.
197 3C). We identified three types of excitatory neurons (ExN: ExN1, ExN2, ExN3), four types of
198 inhibitory neurons (InN: InN1, InN2, InN3, InN4), two types of oligodendrocytes (Oligo and
199 Oligo2), oligodendrocyte precursor cells (OPC), astrocytes (Astro), and microglia (MG) (Fig. 3D).
200 Vascular endothelial cells (Vasc) were also identified but were not further studied. The
201 characteristic marker gene expression for each cell cluster is shown in Supp. Fig. 3C-G.
202 Expression in all ExNs is consistent with pyramidal neurons. In ExN1, differential expression was
203 consistent with large layer 5 pyramidal neurons shown e.g. by *Fezf2* expression (Fig. 3D, Supp.
204 Fig. 3D, F-G)). In the largest ExN subcluster, ExN2, differential expression was consistent with
205 pyramidal neurons from several neocortical layers. The InN subclusters collectively express
206 several classical InN markers, such as *Vip*, *Sst*, *ErbB4*, while the subclusters InN1 and InN3
207 specifically contain layer 2/3 interneurons (Supp. Fig. 3C). Typical marker signatures used for
208 Oligo and Oligo2 (*Mbp*, *Ptgds*, *Mal*), suggests that Oligo2 also contains minor neuronal
209 populations in addition to oligodendrocytes (Supp. Fig. 3C). The OPC (*Vcan*, *Epn2*, *Tnr*), Astro
210 (*Aqp4*, *Prex2*, *Luzp2*) and MG (*Cd74*, *C1qa*, *Csf1r*) markers are consistent with prior literature^{31,32}.
211 The relative proportions of major cell types were roughly similar between the four genotypes (Fig.
212 3E).

213 Next, we examined the expression of endogenous Gba, mouse Snca in WT brains and the
214 expression of human transgenic SNCA (hSNCA) using Thy-1 in SNCA tg brains (Supp. Fig. 3H-
215 J). Snca is enriched in excitatory neuronal clusters, including ExN1, consistent with published
216 literature (Supp. Fig. 3H)^{33,34}. This pattern was also true for hSNCA³⁴⁻³⁶, although hSNCA is also
217 expressed in glial cell types in SNCA tg mice (Supp. Fig. 3H, I). The high hSNCA expression in
218 the predominantly layer 5-populated ExN1 cluster (Supp. Fig. 3H) is consistent with the layer 5
219 specific increases of α -synuclein pathology demonstrated by immunohistochemistry (Fig. 2H,

220 Supp. Fig. 2A). In contrast, *Gba* is generally found at low levels in brain cells³⁷⁻³⁹ (Supp. Fig. 3J, i
221 and ii).

222
223 **Mutant *Gba* drives transcriptional downregulation of synaptic pathways in neurons:** After
224 correcting for genome-wide comparisons, we identified up- and down-regulated differentially
225 expressed genes (DEGs) in all cell types in *Gba*, *Gba*-SNCA and SNCA tg mice cortices
226 compared with WT (Fig. 3F, Supp. Table 1-3). To gain insights into the cognitive deficits seen in
227 *Gba* mice, we focused on DEGs in neuronal clusters, comparing *Gba* with WT (Supp. Table 1).
228 Strikingly, *Gba* mutant mice showed a general downregulation of many genes functioning at the
229 synapse (*Arc*, *Syp*, *Actb*, *Nrg1*, *Nlgn1*, *Nrg1*, *Grm7*, *Grip1*, *Ptprd*, *Nlgn1*, *Il1rapl2*, *Gabra1*, *Cntn5*,
230 *Lingo2*, *ErbB4*, *Nptn*, *Lrrtm4*, *Actb*, *Cntnap2*, *Lrfn5*), suggestive of a synaptic dysregulation
231 signature related to *Gba*. *Ahi1*, a gene important for cortical development and vesicle trafficking
232 was upregulated in all neuronal classes in *Gba* mice.

233
234 To define the major pathways impacted, we performed unbiased gene ontology (GO) enrichment
235 analysis comparing *Gba* to WT (Fig. 3G, I). As shown by heatmaps depicting the top biological
236 pathway changes, we found a consistent decrease in synaptic pathways in cortical ExNs of *Gba*
237 mice driven by reduced expression of *Syp*, *Actg1*, *Actb*, *Nlgn1*, *Grm8*, *Nrg1*, *Arc* (Fig. 3G). ExN1
238 and ExN2, shared robust downregulation of genes involved in SVE, presynaptic endocytosis, and
239 vesicle-mediated transport in synapse in *Gba* mice (Fig. 3G, highlighted, Supp. Table 4).
240 Additionally, in *Gba* mice, ExN1 and ExN2 showed downregulation of cellular pathways and
241 genes involved in both pre- and postsynapse organization, and synaptic protein-containing
242 complex localization (Fig. 3G, highlighted, Supp. Table 4). In the smaller ExN3 cluster, DEGs
243 were fewer and involved in lysosomal lumen acidification (Supp. Table 4). In contrast, the
244 significant upregulated pathways in ExN1 and ExN2 of *Gba* involve RNA splicing (Fig. 3I, Supp.
245 Table 4). Inhibitory neurons (InN1-4) in *Gba* mutant mice showed downregulation of multiple
246 synapse-associated pathways, including genes involved in synapse organization, synapse
247 membrane adhesion in InN1, synapse assembly in InN4, Wnt signaling in InN2, and
248 axonogenesis (Fig. 3G, Supp. Table 4). The upregulated pathways in InN1-4, similar to ExNs, are
249 related to RNA splicing (Fig. 3I, Supp. Table 4).

250
251 Next, we compared DEGs in neuronal clusters in *Gba*-SNCA with WT (Supp. Table 2). Consistent
252 with our finding of a *Gba*-driven synapse effect, ExN clusters in *Gba*-SNCA mice show robust
253 downregulation of synapse related genes (Supp. Table 4). GO enrichment analysis comparing
254 *Gba*-SNCA to WT revealed the top downregulated pathways in cortical ExN1 and ExN2 were SV
255 cycle, vesicle-mediated transport in synapse, and SVE (driven by *Actb*, *Actg1*, *Unc13a*, *Cacna1a*,
256 *Calm1*, *Btbd9*, *Prkcg*, *Pacsin1* reductions Fig. 3H, highlighted). Although the individual DEGs
257 between *Gba* and *Gba*-SNCA are not identical, the synaptic pathways being impacted are highly
258 similar, suggestive of a common synaptic dysregulation signature related to *Gba* (Compare Fig.
259 3G with 3H). In *Gba*-SNCA InNs we see distinct pathways such as ubiquitin-protein transferase
260 activator activity in InN1 and tRNA aminoacylation in InN2-4 being down regulated (Fig. 3H). The
261 upregulated pathways in *Gba*-SNCA in ExNs are related to focal adhesion assembly and in InNs
262 are diverse and include amyloid binding (Fig. 3J).

263
264 Next, we analyzed all neuronal DEGs through SynGO to define synaptic DEGs in *Gba* and *Gba*-
265 SNCA mice. The SynGO analysis revealed more significant suppression of synaptic genes in ExN
266 classes compared to InN classes in both genotypes (Fig. 4A-D). Cnet plots revealed enrichment
267 of converging and predominantly down-regulated synaptic genes and pathways in both *Gba* and
268 *Gba*-SNCA mouse cortices (Fig. 4E, F), consistent GO analyses (Compare Fig. 3G, H, with Fig.
269 4E, F).

270

271 To evaluate if the downregulation of synapse organization pathways leads to a decrease in
272 excitatory synapse number, we performed electron microscopy on 12-month old cortex samples.
273 Electron microscopy was chosen as it allows for accurate quantification of synapse numbers while
274 avoiding problems of individual synaptic protein marker differences across genotypes. As seen in
275 Fig. 4G-H, number of excitatory synapses in deep layers of cortex is indeed reduced in *Gba*
276 mutant and *Gba*-SNCA mice compared to SNCA and WT mice.

277
278 To assess SVE changes at the protein level, we immunostained cortex and hippocampus
279 sections, for the SVE protein, endophilin A1 (a risk allele for PD) and the endocytic lipid PIP2.
280 Conforming with the snRNA expression data, endophilin A1 and PIP2, showed a decreased trend
281 in the cortex (Fig. 5A, Cortex, B, C). Interestingly, in the synaptic layer in CA1 of the hippocampus
282 where endophilin A1 and PIP2 are enriched, we noted significantly reduced endophilin A1 and
283 PIP2 expression in *Gba* and *Gba*-SNCA mice (Fig. 5A, CA1 hippocampus, D, E). Together, these
284 observations corroborate our findings from snRNA-seq analysis of *Gba*-driven suppression of
285 SVE genes and show these deficits are not limited to the cortex.

286
287 To determine whether these transcriptional and protein expression changes affect the SV cycle,
288 we examined electron micrographs of excitatory synapses in the cortical layer 5/6 and quantified
289 SVs and clathrin coated vesicles (CCVs), which serve as proxies for SV cycling and SVE (Fig.
290 5F-I). In the *Gba* mutant mice, the number of SVs was comparable to that in WT mice, however,
291 a significant loss of CCVs was observed, potentially indicating a slowdown in clathrin-mediated
292 SVE (Fig. 5F-H). In *Gba*-SNCA mice, there was a marked reduction in both SVs and CCVs (Fig.
293 5F-H), with several synapses showing SVs with variable shapes and sizes (Fig. 5F, v), indicating
294 a severe disruption of SVE and SV recycling. Interestingly, the SNCA tg mice displayed a
295 significant increase in CCVs (Fig. 5F and H), consistent with findings in other α -synuclein
296 models^{40,41}. Together, these findings reveal a distinct pattern of SVE disruption in *Gba* mutant
297 mice, which is exacerbated in *Gba*-SNCA mice, with altered SV recycling potentially leading to
298 cognitive dysfunction.

299
300 **ExN1 cluster contains vulnerable layer 5 cortical neurons:** As cortical layer 5 neurons
301 exhibited the highest vulnerability in terms of α -synuclein pathology, (Fig. 2A, H, Supp. Fig. 2A),
302 and transcriptional changes associated with SVE (Fig. 3G, H), we further investigated the ExN1
303 cluster which has high hSNCA transgene and *Gba* expression (Supp. Fig. 3I, J). Upon
304 subclustering, ExN1 was divided into six subclusters (Supp. Fig. 4A-D), all of which contained
305 cells expressing the layer 5 marker *Fezf2* (Supp. Fig. 4D, E). One subcluster, ExN1.1, was
306 characterized by high expression of *Arc* (Supp. Fig. 4D), which is downregulated in *Gba* mutant
307 neurons (Supp. Fig. 4F). Our analysis confirmed the greatest downregulation of synapse-
308 associated genes in ExN1.1 subcluster in both *Gba* and *Gba*-SNCA mice (Supp. Fig. 4D, F-I). In
309 contrast, non-synaptic DEGs were evenly up- and downregulated (Supp. Fig. 4F, G). SV cycle
310 pathways were consistently downregulated throughout ExN1, largely driven by the same genes
311 identified in our non-targeted analysis (Fig. 3G, H). Additionally, *Rab26*, a key regulator of SV
312 endocytosis and autophagy⁴², was downregulated in both *Gba* genotypes (Supp. Fig. 4H, I).
313 These findings suggest that layer 5 excitatory neurons are selectively vulnerable because of both
314 high hSNCA and *Gba* expression and SV cycling deficits driven by *Gba* mutations. These
315 mechanisms appear to act synergistically to exacerbate α -synuclein pathology in *Gba*-SNCA
316 mice.

317
318 **Modest glial transcriptional changes in *Gba* mutant and *Gba*-SNCA cortex:** Compared to
319 neuronal clusters, glial clusters in *Gba* and *Gba*-SNCA cortices exhibited fewer DEGs (Fig. 3F,
320 Supp. Table 1-3). In *Gba* cortex, MG showed altered gene expression patterns indicative of
321 reduced synaptic remodeling. Notably, synapse pruning and regulation of SV clustering pathways

322 were downregulated (Fig. 3G, Table 4). Postsynaptic neurotransmitter receptor diffusion trapping
323 was upregulated (Fig. 3I, Supp. Table 4). These changes reinforce synapse dysfunction as a
324 central pathological mechanism in *Gba* mutant cortex. The down and upregulated pathways in
325 astrocytes in *Gba* are related to cellular extravasation and morphology (Fig. 3I, Supp. Table 4).
326 There were fewer DEGs in OPCs and Oligodendrocytes (Fig. 3F); therefore, clear pathway
327 differences are harder to discern (Fig. 3G-I).

328
329 In *Gba*-SNCA, MG exhibit decreased endoplasmic reticulum stress response, while SNARE
330 binding and aspects of phosphatidylinositol binding were upregulated (Fig. 3H, J, Supp. Table 4).
331 *Gba*-SNCA Astro exhibit decreased tRNA aminacylation and increased amyloid-beta binding (Fig.
332 3H, J). In *Gba*-SNCA OPCs, phosphatidylinositol binding was downregulated, while
333 Oligodendrocytes showed modest pathway changes (Fig. 3H, J). Overall, in *Gba* mice, all glial
334 cell types have muted responses, while *Gba*-SNCA mice had slight astrocytic activation. To
335 confirm our analysis, we immunostained with the microglial marker Iba1, CD68 for activated
336 microglia, and GFAP for astrocytes (Supp. Fig. 5). We did not observe any significant increase in
337 Iba1 or CD68+ve microglial number, suggesting negligible microglial activation in *Gba* and *Gba*-
338 SNCA cortex. We observed a trend towards increased GFAP levels in *Gba*-SNCA mice compared
339 to WT (Supp. Fig. 5A-D). Together, these data suggest that glial responses are modest,
340 consistent with snRNAseq data.

341 **Cortical transcriptional changes indicate broad synapse dysregulation in SNCA cortex:**
342 SNCA tg mice showed the greatest number of DEGs compared to WT relative to *Gba* and *Gba*-
343 SNCA mice (Fig. 3F, Supp. Table 3). The neuronal clusters showed broad alterations of synapse
344 related gene expression. Both up and down-regulated DEGs are involved in synapse assembly,
345 regulation of synapse structure or activity, and postsynapse organization (Supp. Figs. 6A-B, Supp.
346 Table 3). SynGO analysis of these DEGs revealed regulation of synapse structure and function
347 as the main pathway impacted in SNCA tg mice (Supp. Fig. 6C-D). As excitatory synapse number
348 was not changed significantly in cortical regions of SNCA tg mice (Fig. 4G, H) compared to WT,
349 this likely results in functional deficits. Consistent with the observed cortical α -synuclein pathology
350 at this age (Fig. 2A, D), unfolded protein handling was upregulated, as were pathways involved
351 in protein folding and refolding specifically in ExN1 and ExN2 clusters (Supp. Fig. 6B, Supp. Table
352 3). Additionally, regulation of protein ubiquitination was upregulated in all ExNs (Supp. Fig. 6B,
353 Supp. Table 3). OPCs and oligodendrocytes show changes related to oligodendrocyte
354 differentiation. MG showed down-regulation in immune receptor binding and up-regulation in
355 cation channel activity (Supp. Fig. 6A-B, Supp. Table 3). In Astros, cell junction assembly was
356 decreased, and ion channel activity was increased (Supp. Fig. 6A-B). However, we did not
357 observe significant microgliosis or astrogliosis in SNCA tg mice cortices by immunohistochemistry
358 (Supp. Fig. 5). Despite SNCA transcriptional changes, *Gba* signatures are predominant in *Gba*-
359 SNCA cortices.

360 **Discussion:**

361 Surveys of PD and DLB patients and their caregivers highlight that maintaining cognitive abilities
362 is a major unmet need⁴³. The *GBA* gene is an ideal choice to investigate this non-motor symptom,
363 because it is the most common risk gene for PD⁸ and *GBA* mutations are linked to cognitive
364 deficits in both diseases^{8,18}. Here, we present detailed age-dependent behavioral and pathological
365 phenotyping of the *Gba*-SNCA line alongside WT, *Gba* mutant, and SNCA tg mice. We
366 demonstrate that *Gba*-SNCA mice recapitulate both cognitive dysfunction and motor deficits seen
367 in *GBA*-linked PD and DLB. Significantly, we carried out snRNA-seq analysis of the cerebral
368 cortex in these four mice genotypes and have built one of the first comprehensive *Gba*

369 transcriptomic data sets. We encourage the scientific research community to utilize this rich
370 dataset as a resource for additional analyses on PD and DLB (NCBI GEO GSE283187).

371 **Gba-SNCA as a mouse model of GBA-linked PD and DLB.** Cognitive dysfunction has been
372 noted in several existing mice models of PD designed to study motor deficits, including those
373 focused on α -synuclein pathology⁴⁴⁻⁴⁷. These models involve overexpression of hSNCA mutations
374 or the use of pre-formed fibrils to induce α -synuclein aggregation⁴⁸ and have been instrumental
375 in elucidating the mechanisms of α -synuclein pathology and its impact on neurodegeneration and
376 cognitive decline. However, they do not fully replicate the complex genetic and pathological
377 features of human PD and DLB, importantly, the contribution of *GBA*. Additionally, most biallelic
378 *Gba* models are hampered by early lethality, precluding age-related studies, and hence
379 investigated as heterozygotes^{48,49}. Here, we build on our previous analyses of long-lived biallelic,
380 *Gba* mutant mice and *Gba*-SNCA²⁶ and show that *Gba*-SNCA mice are an excellent model of
381 GBA-linked PD and DLB. *Gba*-SNCA mice offer significant advancements as they exhibit
382 worsened motor deficits compared to SNCA tg in an age-dependent manner as well as early
383 cognitive deficits, closely mirroring the human condition. This is further evidenced by exacerbation
384 of cortical α -synuclein pathology in *Gba*-SNCA mice. Significantly, by comparing *Gba*, SNCA tg,
385 and *Gba*-SNCA mice, we were able to demonstrate that the *Gba* mutation alone can drive
386 cognitive dysfunction. These data are congruent with recent studies using heterozygous L444P
387 *Gba* mutant mice^{49,50}. Notably, *Gba*-SNCA mice exhibited enhanced motor deficits, but cognitive
388 deficits were on par with *Gba* mice, matching the similar synaptic pathway deficits in their neuronal
389 populations as assessed by snRNAseq. In sum, *Gba*-SNCA mice capture the complexities of
390 GBA-linked PD and DLB and serve as a good mouse model for these synucleinopathies.

391
392 **GBA-linked cognitive dysfunction is independent of α -synuclein pathology.** A striking
393 finding is that cognitive dysfunction occurs independent of or precede α -synuclein pathology in
394 *Gba* mutants. pSer129 α -syn is the gold standard to define Lewy bodies in both PD and DLB⁵¹⁻⁵⁷
395 ^{56,58,59}. Yet, we did not detect any pSer129 α -syn in *Gba* mutant brain nor did we observe
396 redistribution of α -synuclein to the soma, a posttranslational modification independent measure
397 of pathology⁶⁰. This was most evident in the hippocampus, where the synaptic and cell body layers
398 are demarcated. While α -synuclein pathology in cortical areas does lead to cognitive dysfunction
399 in mice overexpressing mutant α -synuclein or those injected with PFFs⁴⁷, our study specifically
400 challenges the necessity of α -synuclein pathology in the development of cognitive deficits in *GBA*
401 mutations. Clinical support for this comes from children with neuropathic forms of Gaucher
402 disease, who show cognitive deficits but do not develop neocortical α -synuclein pathology^{61,62}.
403 While a recent study has made similar observations focusing on the hippocampus⁵⁰, it would be
404 interesting to explore whether aging *Gba* mice could initiate α -synucleinopathy or if other
405 pathological forms of α -synuclein are involved.

406
407 In contrast to cognitive deficits, motor deficits are strongly related to α -synuclein pathology in *Gba*-
408 SNCA mice. Notably, we observed significant α -synuclein pathology in cortical layers 5, similar to
409 that seen in other PD mice models and human PD and DLB patients^{34,63}. Our snRNA-seq data
410 suggest that layer 5 ExNs are also vulnerable to *Gba* mediated synaptic dysfunction, which could
411 contribute to an increased accumulation of α -synuclein pathology in cortical layer 5, and in turn,
412 the severity of the motor deficits. Thus, *Gba*-SNCA mice also highlight specific cortical neuronal
413 vulnerabilities, allowing for further investigations into cortical mechanisms of PD and DLB.

414
415 **SVE and organization deficits in *Gba*-linked cognitive dysfunction.** Our snRNAseq analysis
416 showed clear evidence of specific synaptic changes. Many synaptic genes that function in SV
417 cycle, SVE, synapse organization, synapse membrane adhesion, and synapse assembly were
418 downregulated in neuronal clusters in the cortex of *Gba* as well as in *Gba*-SNCA mice, suggesting

419 common synaptic dysfunction mechanisms linked to *Gba*. Because *Gba* mutant mice do not show
420 α -synuclein pathology, this implies that synaptic dysfunction directly contributes to the observed
421 cognitive deficits, rather than a consequence of disease pathology or neurodegeneration. In
422 support of this tenet, we observed excitatory neuronal synapse loss in the cortex of *Gba* mutant
423 and *Gba*-SNCA mice. In other dementias such as Alzheimer's disease, synapse loss correlates
424 tightly with cognitive decline⁶⁴. Our findings suggest that this is likely true for GBA-linked PD and
425 DLB, in line with available clinical studies⁶⁵⁻⁶⁷.

426
427 SVE was the major pathway downregulated in neurons in both *Gba* mutant and *Gba*-SNCA mice,
428 supported by our immunohistochemistry and electron microscopy experiments. Three key genes
429 driving this pathway are *Hspa8*, *Dlg2* and *Arc*. *Hspa8* (encoding HSC70) contributes to synapse
430 vesicle uncoating and functions with *Dnajc6/PARK19*, a familial PD gene^{28,68}. *Dlg2* is a risk gene
431 for sporadic PD that participates in receptor clustering in synapses⁶⁹. *Arc* is an activity regulated
432 gene that regulates transcription of many synaptic and SVE genes⁷⁰. Interestingly, both clinical
433 and experimental data link SVE deficits to cognitive deficits. The levels of dynamin1, the endocytic
434 GTPase, correlate with Lewy Body Dementia⁷¹. Patients with mutations in *DNAJC6/PARK19* and
435 *Synj1/PARK20* which encode two key SVE proteins--auxilin and synaptojanin1—have cognitive
436 deficits. Endocytic mutant mice show deficits in NOR and fear conditioning^{72,73}, supporting the
437 tenet that SVE deficits lead to cognitive dysfunction. We suggest that *Arc* could serve as an
438 upstream regulator of the synaptic transcriptional changes seen in *Gba* and *Gba*-SNCA cortices.
439 Another contributor to the *Gba*-driven alteration of SV cycling is plasma membrane lipid
440 composition changes. Emerging evidence indicates altered sphingolipid composition, such as in
441 *Gba* mutants, may interfere with phosphoinositide biology at membranes^{74,75}. Future research
442 should address the topic of co-regulated lipids.

443
444 **Limitations:** The *Gba*-SNCA mouse model effectively replicates both behavioral and
445 histopathological characteristics of GBA-linked PD and DLB, offering a valuable tool for future
446 research. Our study highlights the critical role of synaptic dysfunction in GBA-linked cognitive
447 decline, occurring independent of α -synuclein pathology. While transcriptional analysis supported
448 by histology revealed significant disruptions in SVE and synapse assembly in cortical excitatory
449 neurons of both *Gba* and *Gba*-SNCA mice, the upstream regulators of these changes remain to
450 be identified. While glial cells exhibit a more modest transcriptional response compared to
451 neurons at this age, their involvement in synaptic dysfunction at earlier stages cannot be ruled
452 out. Our comprehensive transcriptomic dataset provides a rich resource for further exploration,
453 and we encourage the scientific community to leverage this data to elucidate GBA-linked disease
454 mechanisms.

455
456 **Methods:**

457 **Mice:** *Gba* mutant mice have been previously described in Mistry et al. (2010)⁷⁶ and Taguchi et
458 al. (2017)²⁶. These mice have a copy of the *Gba* L444P mutant allele and a *Gba* KO allele, with
459 *Gba* expression rescued in skin to prevent early lethality. SNCA tg mice overexpress the human
460 α -synuclein A30P transgene (heterozygous), and have also been previously described³⁰. *Gba*
461 mutant mice were crossed to SNCA tg to obtain *Gba*-SNCA double mutant mice. Age and sex
462 matched WT mice were used controls.

463 **Behavior evaluation:** WT, *Gba*, SNCA tg, and *Gba*-SNCA mice were examined for motor
464 behavior longitudinally at 3, 6, 9, and 12 months of age as described previously (n=9-12
465 mice/genotype, sex-matched)²⁹. The balance beam test assesses the ability to walk straight on a
466 narrow beam from a brightly lit end towards a dark and safe box. Number of times a mouse could
467 perform this behavior in a minute and the average time taken for each run were evaluated. The

468 grip strength of all the limbs and the forelimbs was assessed by measuring the maximum force
469 (g) exerted by the mouse in grasping specially designed pull bar assembly in tension mode,
470 attached to a grip strength meter (Columbus Instruments, Ohio, USA). Mice, when picked up by
471 the base of the tail and lowered to a surface, extend their limbs reflexively in anticipation of
472 contact. Mice with certain neurological conditions display hind limb clasp instead of extension.
473 Mice were tested on this maneuver for 30 secs and the hindlimb, forelimb, and trunk clasps were
474 scored (0: no clasp; 1: one hind limb clasp; 2: both the hind limbs clasp; 3: Both the hind limbs
475 clasping with at least one forelimb clasp; 4: Both the hind limbs clasp with trunk clasping). For
476 evaluation of overall locomotory capabilities, mice were allowed to explore an open field arena for
477 5 minutes, which was videotaped to assess the distance travelled using Noldus Ethovision CT
478 software.

479 To evaluate cognition, we employed fear conditioning and novel object recognition (NOR) tests.
480 To avoid learning-induced confounding factors, we performed these tests on two separate sets of
481 mice at 3 and 12 months. For fear conditioning test, we initially habituated mice in standard
482 operant boxes for 2 minutes, followed by exposure to a 30-second neutral stimulus (a 80 dB tone),
483 which ended with 2 seconds of an aversive stimulus (a 0.1 to 1.0 mA electric shock). This pairing
484 associates the neutral stimulus with fear, leading the mice to exhibit fear responses, such as
485 freezing, when exposed to the tone alone. We tested for freezing 24 hours later on the testing
486 day. Cognitively normal mice will form a conditioned fear response, exhibiting increased freezing
487 behavior on the testing day compared to the training day after exposure to the tone alone,
488 indicating their ability to associate tone with the electric shock they received on the training day.
489 We measure this conditioned fear response as the number of freeze counts after starting the tone
490 for a total of 3 minutes. The NOR test was used to assess the recognition memory. First, mice
491 were acclimatized to the novel object arena without any objects in it. After 24 hours, familiarization
492 session was performed where mice were presented with two similar objects for 8 minutes. After
493 18-20 hours, one of the two objects was replaced by a novel object and mice were allowed to
494 explore for 8 minutes. Mice being exploratory animals, spend more time with novel object when
495 their cognition is normal, which we used as a measure of NOR test.

496 **Immunohistochemistry:** Equal number of male and female mice at 3 and 12 months of age
497 (n=3-6/genotype) were used for immunohistochemistry. Mice were anaesthetized using isoflurane
498 inhalation and perfused intracardially with chilled 0.9 % heparinized saline followed by chilled 4
499 % paraformaldehyde (PFA) in 0.1 M phosphate buffer (PB). The brains were post-fixed in the
500 same buffer for ~48 hours and cryoprotected in increasing grades of buffered sucrose (15 and 30
501 %, prepared in 0.1 M PB), at 4 °C, and stored at -80 °C until sectioning. Sagittal brain sectioning
502 (30 µm thick) was performed using a cryostat (Leica CM1850, Germany), and the sections were
503 collected on gelatinized slides, and stored at -20 °C until further use. For immunofluorescence
504 staining, sections were incubated in 0.5 % triton-X 100 (Tx) (15 mins), followed by incubation in
505 0.3 M glycine (20 mins). Blocking was performed using 3% goat serum (90 mins), followed by
506 overnight incubation (4° C) in the primary antibodies. Following day, sections were incubated in
507 Alexa-conjugated secondaries for 3-4 hours, followed by coverslip mounting using an antifade
508 mounting medium with (H-1000, Vectashield) or without (H-1200, Vectashield) DAPI. Coverslips
509 were sealed using nail polish. 1X PBS with 0.1 % Tx was used as both washing and dilution
510 buffer. Below is the list of antibodies used and their dilutions.

511

Antibody	Dilution	Manufacturer, RRID
Mouse Anti- α -Synuclein	1:500	BD Biosciences (610786), AB_398107
Guinea Pig Anti-NeuN	1:500	Sigma-Aldrich (ABN90P), AB_2341095
Rabbit Anti- α -synuclein (phospho S129)	1:800	Abcam (ab51253), AB_869973
Rabbit Anti-Iba1	1:300	Wako Chemicals (019-19741), AB_839504

Guinea Pig Anti-GFAP	1:400	Synaptic Systems (173004), AB_1064116
Mouse Anti-CD68	1:400	Invitrogen (MA1-80557), AB_929627
Rabbit Anti-Endophilin 1	1:200	Synaptic Systems (159002), AB_887757
Mouse Anti-PIP2	1:200	Invitrogen (MA3-500), AB_568690

512 **Fluorescence slide scanner, confocal microscopy, and image analysis:** Fluorescent images
513 were acquired using a fluorescence slide scanner (VS200, Olympus) or confocal microscope
514 (LSM 800, Zeiss) with a 40X objective using appropriate Z-depth. Images were then analyzed
515 using FIJI software from National Institute of Health (NIH), blinded for genotype. Whole cortex
516 was demarcated as per Paxinos and Franklin, 2008. After performing sum intensity projection,
517 the expression intensity was measured on an 8-bit image as the mean gray value on a scale of
518 0–255, where '0' refers to minimum fluorescence and '255' refers to maximum fluorescence. For
519 counting NeuN+ neurons, images were thresholded using the 'otsu' algorithm and the cells larger
520 than 25 μm^2 were counted using the 'analyze particles' function²⁹. A similar method was used to
521 count Iba1+ve microglial cells, and CD68 +ve cells. GFAP+ astroglial cells were counted manually
522 using the 'cell counter' function. Regions of interest (ROIs) obtained for individual NeuN+ were
523 overlaid on pSer129 α -syn staining to obtain numbers of neurons that were positive for
524 pSer129 α -syn. To analyze the cortical layer-specific expression of α -synuclein and pSer129 α -
525 syn, we initially determined the proportions of cortical layers (1 to 6b) in sagittal brain slice images
526 obtained from the Allen Brain Atlas (<https://mouse.brain-map.org/>). This involved drawing
527 perpendicular lines across cortical layers using FIJI software. Proportions were calculated across
528 three different sample areas of the entire cortex. Intensity profiles for α -synuclein and pSer129 α -
529 syn expression across cortical layers were then generated by drawing perpendicular lines and
530 utilizing the "RGB Profile Plot" function on FIJI for the corresponding sample areas. The resulting
531 expression values, scaled from 0 to 255, were subsequently assigned to the proportions of layers
532 1 to 6b obtained from the Allen Brain Atlas.

533 **Electron Microscopy:** Brains of 12-month-old mice (n=2-3 per genotype) were fixed via
534 intracardial perfusion with a solution of 2% PFA and 2% glutaraldehyde in 0.1M PB. This was
535 followed by an overnight immersion in 0.1M cacodylate buffer containing 2.5% glutaraldehyde
536 and 2% PFA²⁹. The cortical layers 5 and 6 were then dissected and processed at the Yale Center
537 for Cellular and Molecular Imaging's Electron Microscopy Facility. Electron microscopy imaging
538 was conducted using an FEI Tecnai G2 Spirit BioTwin Electron Microscope, and the resulting
539 micrographs were analyzed for excitatory asymmetric synapses, their synaptic vesicles and
540 clathrin coated vesicles using FIJI software, with the analysis performed blind to genotype.

541 **Nuclei isolation from cerebral cortex:** Fresh cortical tissue were dissected from left hemisphere
542 of 12 month old WT, Gba, SNCA tg and Gba-SNCA mice after euthanasia. Single nuclei were
543 isolated as previously described with modifications³¹. All procedures were carried out on ice or at
544 4°C. Briefly, fresh cortical tissue was homogenized in 8.4 ml of ice-cold nuclei homogenization
545 buffer [2 M sucrose, 10 mM Hepes (pH 7.5), 25 mM KCl, 10% glycerol, 1 mM EDTA (pH 8.0), and
546 ribonuclease (RNase) inhibitors freshly added (40U/ml)] using a Wheaton Dounce tissue grinder
547 (10 strokes with the loose pestle and 10 strokes with the tight pestle). The homogenate was
548 carefully transferred into a 15 ml ultracentrifuge tube on top of 5.6 ml of fresh nuclei
549 homogenization buffer cushion and centrifuged at 25,000 rpm for 60 min at 4°C in an
550 ultracentrifuge. The supernatant was removed, and the pellet was resuspended in 1 ml of nuclei
551 resuspension buffer [15 mM Hepes (pH 7.5), 15 mM NaCl, 60 mM KCl, 2 mM MgCl₂, 3 mM CaCl₂,
552 and RNase inhibitors freshly added (40U/ml)] and counted on a hemocytometer with Trypan Blue
553 staining. The nuclei were centrifuged at 500g for 10 min at 4°C with a swing bucket adaptor. They
554 were subsequently resuspended at a concentration of 700 to 1200 nuclei/ μl in the nuclei
555 resuspension buffer for the next step of 10x Genomics Chromium loading and sequencing.

556 **Droplet-based single nucleus RNA sequencing and data alignment:** After quality control, we
557 recovered a total of 104,750 nuclei, including 31,906 nuclei from WT, 28,568 from Gba mutant,
558 26,579 from SNCA tg, and 17,697 from Gba-SNCA cortices. The mean reads per nuclei was
559 34,312 and the median number of identified genes per nuclei was 2410 in all samples. The
560 snRNA-seq libraries were prepared by the Chromium Single Cell 3' Reagent Kit v3.1 chemistry
561 according to the manufacturer's instructions (10x Genomics). The generated snRNA-seq libraries
562 were sequenced using Illumina NovaSeq6000 S4 at a sequencing depth of 300 million reads per
563 sample. For snRNA-seq of brain tissues, a custom pre-mRNA genome reference was generated
564 with mouse genome reference (available from 10x Genomics) that included pre-mRNA
565 sequences, and snRNA-seq data were aligned to this pre-mRNA reference to map both unspliced
566 pre-mRNA and mature mRNA using CellRanger version 3.1.0. The raw data are available on
567 NCBI GEO GSE283187 (<https://www.ncbi.nlm.nih.gov/geo/query/acc.cgi?acc=GSE283187>).

568 **Single-cell quality control, clustering, and cell type annotation:** After quality control filtering
569 by eliminating nuclei with less than 200 genes or more than 5% mitochondrial gene expression
570 (poor quality nuclei) or more than 6,000 genes (potential doublets) per nucleus, we profiled
571 104,750 brain nuclei. Seurat (version 4.2.0) single cell analysis R package was used for
572 processing the snRNA-seq data. The top 2000 most variable genes across all nuclei in each
573 sample were identified, followed by the integration and expression scaling of all samples and
574 dimensionality reduction using principal components analysis (PCA). Uniform Manifold
575 Approximation and Projection for Dimension Reduction (UMAP) was then applied to visualize all
576 cell clusters, and the classification and annotation of distinct cell types were based on known
577 marker genes of each major brain cell type and the entire single nucleus gene expression matrix
578 were investigated but were not used in downstream analyses.

579 **Differential expression (DE) analysis:** Differential expression analysis for snRNA-seq data was
580 performed using the Wilcoxon Rank Sum test using the function FindMarkers of the Seurat
581 package (4.1.0) in R. For all cells, the threshold for differentially expressed genes (DEGs) was
582 set as the expression log₂ fold change of Mutant/WT mice being greater than 0.2 and significantly
583 changed ($p < 0.05$) after Bonferroni (BF)-correction for multiple comparisons and adjustment for
584 possible confounders, using default parameters. Adjustment was made for differences in sex,
585 batch and read depth with MAST⁷⁷.

586 **Gene ontology (GO) pathway and targeted gene expression analysis.** Gene-set and protein
587 enrichment analysis was performed using the function enrichGO from the R package
588 clusterProfiler in Bioconductor (3.14)⁷⁸, with the DEGs that were significant after correction (see
589 above) as input. Cnet plots were produced using the same package. The top three GO terms from
590 biological process (BP) based on the lowest p-value were identified and plotted in a heatmap,
591 without selection. Molecular function (MF) subontologies were shown instead of BP in a few cases
592 (< 8) where BP contained duplicates or triplicates of the same pathway, for illustrative purposes,
593 with the same DEGs and ranking used for BP and MF subontologies. The background genes
594 were set to be all the protein-coding genes for the mouse reference genome. Default values were
595 used for all parameters. In GO pathway analysis DEGs were entered only if significant after
596 genome-wide BF correction (for the total number of expressed genes), using Seurat default
597 settings, and in targeted analyses of genes of interest – i.e., genes known to function in the
598 synapse as defined by the SynGO consortium (<https://syngoportal.org>)- after BF correction for the
599 number of investigated genes. For the latter analysis, 1203 genes were found expressed in the
600 dataset.

601 **Statistics:** For motor behavioral studies, two-way repeated measure ANOVA followed by Sidak's
602 multiple comparison test was used. For cognitive behavior assays, one-way ANOVA followed by
603 Sidak's multiple comparison tests or Student's t-test with Welch's correction was used. For

604 immunohistochemistry experiments, one-way ANOVA followed by Sidak's multiple comparison
605 tests was used.

606 **Acknowledgement:** This research was funded by National Institute of Health (NIH-NINDS,
607 1RF1NS110354-01) R01 grant, Bell Research Initiative for Patients with Parkinson's Disease,
608 and Parkinson's Foundation Research Center of Excellence (PF-RCE-1946) grant to S.S.C, US
609 Department of Defense Early Investigator Research award (W81XWH-19-1-0264) to D.J.V., and
610 in part by the Michael J. Fox Foundation for Parkinson's Research (MJFF-020160) to S.S.C. and
611 D.J.V. D.J.V.. We thank the Yale Neuroscience Rodent Behavior Analysis facility and Yale
612 Neuroscience Imaging Core supported by The Kavli Institute of Neuroscience for usage of their
613 microscopes. We thank Betül Yücel for contributing to genotyping of SNCA tg mice.

614

615 **Conflicts of interest:** Authors have no conflicts of interest to declare.

616

617 **Author Contribution:** D.J.V., D.B., and S.S.C. conceptualized the study. D.J.V. conducted
618 behavioral experiments and analyzed the data, prepared samples for histology and Western
619 blotting, and performed immunohistochemistry, imaging, and image analyses. D.B. prepared
620 samples for snRNA-seq and analyzed the snRNA-seq data. R.C. analyzed behavioral data and
621 performed immunohistochemistry, Western blotting, imaging, and image analyses. J.R. set up
622 founder breeding colonies and conducted genotyping for Gba L444P/KO and Gba-SNCA mice.
623 J.P. assisted with snRNA-seq data analysis. P.M. contributed to the initial conceptualization of
624 the study and provided founder colonies of Gba L444P/KO mice. D.J.V., D.B., and S.S.C. wrote
625 the manuscript. All authors have read and contributed to the manuscript.

626

627 **References:**

- 628 1. Bultron, G., *et al.* The risk of Parkinson's disease in type 1 Gaucher disease. *J Inherit Metab*
629 *Dis* **33**, 167-173 (2010).
- 630 2. Sidransky, E., *et al.* Multicenter analysis of glucocerebrosidase mutations in Parkinson's
631 disease. *N Engl J Med* **361**, 1651-1661 (2009).
- 632 3. Aharon-Peretz, J., Rosenbaum, H. & Gershoni-Baruch, R. Mutations in the
633 glucocerebrosidase gene and Parkinson's disease in Ashkenazi Jews. *N Engl J Med* **351**,
634 1972-1977 (2004).
- 635 4. Shiner, T., *et al.* High Frequency of GBA Gene Mutations in Dementia With Lewy Bodies
636 Among Ashkenazi Jews. *JAMA Neurol* **73**, 1448-1453 (2016).
- 637 5. Tsuang, D., *et al.* GBA mutations increase risk for Lewy body disease with and without
638 Alzheimer disease pathology. *Neurology* **79**, 1944-1950 (2012).
- 639 6. Siebert, M., Sidransky, E. & Westbroek, W. Glucocerebrosidase is shaking up the
640 synucleinopathies. *Brain* **137**, 1304-1322 (2014).
- 641 7. Aarsland, D., *et al.* Parkinson disease-associated cognitive impairment. *Nat Rev Dis Primers*
642 **7**, 47 (2021).
- 643 8. Liu, G., *et al.* Specifically neuropathic Gaucher's mutations accelerate cognitive decline in
644 Parkinson's. *Ann Neurol* **80**, 674-685 (2016).
- 645 9. Mata, I.F., *et al.* GBA Variants are associated with a distinct pattern of cognitive deficits in
646 Parkinson's disease. *Mov Disord* **31**, 95-102 (2016).
- 647 10. Tsuji, S., *et al.* A mutation in the human glucocerebrosidase gene in neuronopathic Gaucher's
648 disease. *N Engl J Med* **316**, 570-575 (1987).
- 649 11. Tsuji, S., *et al.* Genetic heterogeneity in type 1 Gaucher disease: multiple genotypes in
650 Ashkenazic and non-Ashkenazic individuals. *Proc Natl Acad Sci U S A* **85**, 2349-2352 (1988).
- 651 12. Charrow, J., *et al.* The Gaucher registry: demographics and disease characteristics of 1698
652 patients with Gaucher disease. *Arch Intern Med* **160**, 2835-2843 (2000).

- 653 13. Grabowski, G.A., Petsko, G.A. & Kolodny, E.H. Gaucher Disease. in *The Online Metabolic*
654 *and Molecular Bases of Inherited Disease* (ed. D.L. Valle, S. Antonarakis, A. Ballabio, A.L.
655 Beaudet & G.A. Mitchell) (McGraw-Hill Education, New York, NY, 2019).
- 656 14. Alcalay, R.N., *et al.* Comparison of Parkinson risk in Ashkenazi Jewish patients with Gaucher
657 disease and GBA heterozygotes. *JAMA Neurol* **71**, 752-757 (2014).
- 658 15. Brockmann, K., *et al.* GBA-associated Parkinson's disease: reduced survival and more rapid
659 progression in a prospective longitudinal study. *Mov Disord* **30**, 407-411 (2015).
- 660 16. Winder-Rhodes, S.E., *et al.* Glucocerebrosidase mutations influence the natural history of
661 Parkinson's disease in a community-based incident cohort. *Brain* **136**, 392-399 (2013).
- 662 17. Oeda, T., *et al.* Impact of glucocerebrosidase mutations on motor and nonmotor complications
663 in Parkinson's disease. *Neurobiol. Aging* **36**, 3306-3313 (2015).
- 664 18. Szewdo, A.A., *et al.* GBA and APOE Impact Cognitive Decline in Parkinson's Disease: A 10-
665 Year Population-Based Study. *Mov Disord* **37**, 1016-1027 (2022).
- 666 19. Alcalay, R.N., *et al.* Glucocerebrosidase activity in Parkinson's disease with and without GBA
667 mutations. *Brain* **138**, 2648-2658 (2015).
- 668 20. Rocha, E.M., *et al.* Progressive decline of glucocerebrosidase in aging and Parkinson's
669 disease. *Ann Clin Transl Neurol* **2**, 433-438 (2015).
- 670 21. Hallett, P.J., *et al.* Glycosphingolipid levels and glucocerebrosidase activity are altered in
671 normal aging of the mouse brain. *Neurobiol. Aging* **67**, 189-200 (2018).
- 672 22. Watson, G.S. & Leverenz, J.B. Profile of cognitive impairment in Parkinson's disease. *Brain*
673 *Pathol* **20**, 640-645 (2010).
- 674 23. Gegg, M.E., *et al.* Glucocerebrosidase deficiency in substantia nigra of parkinson disease
675 brains. *Ann Neurol* **72**, 455-463 (2012).
- 676 24. Zunke, F., *et al.* Reversible Conformational Conversion of α -Synuclein into Toxic Assemblies
677 by Glucosylceramide. *Neuron* **97**, 92-107.e110 (2018).
- 678 25. Mazzulli, J.R., *et al.* Gaucher disease glucocerebrosidase and α -synuclein form a bidirectional
679 pathogenic loop in synucleinopathies. *Cell* **146**, 37-52 (2011).
- 680 26. Taguchi, Y.V., *et al.* Glucosylsphingosine Promotes α -Synuclein Pathology in Mutant GBA-
681 Associated Parkinson's Disease. *J Neurosci* **37**, 9617-9631 (2017).
- 682 27. Straniero, L., *et al.* The SPID-GBA study: Sex distribution, Penetrance, Incidence, and
683 Dementia in GBA-PD. *Neurol Genet* **6**, e523 (2020).
- 684 28. Vidyadhara, D.J., Lee, J.E. & Chandra, S.S. Role of the endolysosomal system in Parkinson's
685 disease. *J. Neurochem.* **150**, 487-506 (2019).
- 686 29. Vidyadhara, D.J., *et al.* Dopamine transporter and synaptic vesicle sorting defects underlie
687 auxilin-associated Parkinson's disease. *Cell Rep* **42**, 112231 (2023).
- 688 30. Chandra, S., Gallardo, G., Fernández-Chacón, R., Schlüter, O.M. & Südhof, T.C. Alpha-
689 synuclein cooperates with CSP α in preventing neurodegeneration. *Cell* **123**, 383-396
690 (2005).
- 691 31. Wang, N., *et al.* Decoding transcriptomic signatures of cysteine string protein alpha-mediated
692 synapse maintenance. *Proc Natl Acad Sci U S A* **121**, e2320064121 (2024).
- 693 32. Zhu, B., *et al.* Single-cell transcriptomic and proteomic analysis of Parkinson's disease Brains.
694 *bioRxiv*, 2022.2002.2014.480397 (2022).
- 695 33. Shwab, E.K., *et al.* Single-nucleus multi-omics of Parkinson's disease reveals a glutamatergic
696 neuronal subtype susceptible to gene dysregulation via alteration of transcriptional networks.
697 *Acta Neuropathol Commun* **12**, 111 (2024).
- 698 34. Goralski, T.M., *et al.* Spatial transcriptomics reveals molecular dysfunction associated with
699 cortical Lewy pathology. *Nat Commun* **15**, 2642 (2024).
- 700 35. Geertsma, H.M., *et al.* A topographical atlas of α -synuclein dosage and cell type-specific
701 expression in adult mouse brain and peripheral organs. *NPJ Parkinsons Dis* **10**, 65 (2024).
- 702 36. Taguchi, K., Watanabe, Y., Tsujimura, A. & Tanaka, M. Brain region-dependent differential
703 expression of alpha-synuclein. *J. Comp. Neurol.* **524**, 1236-1258 (2016).

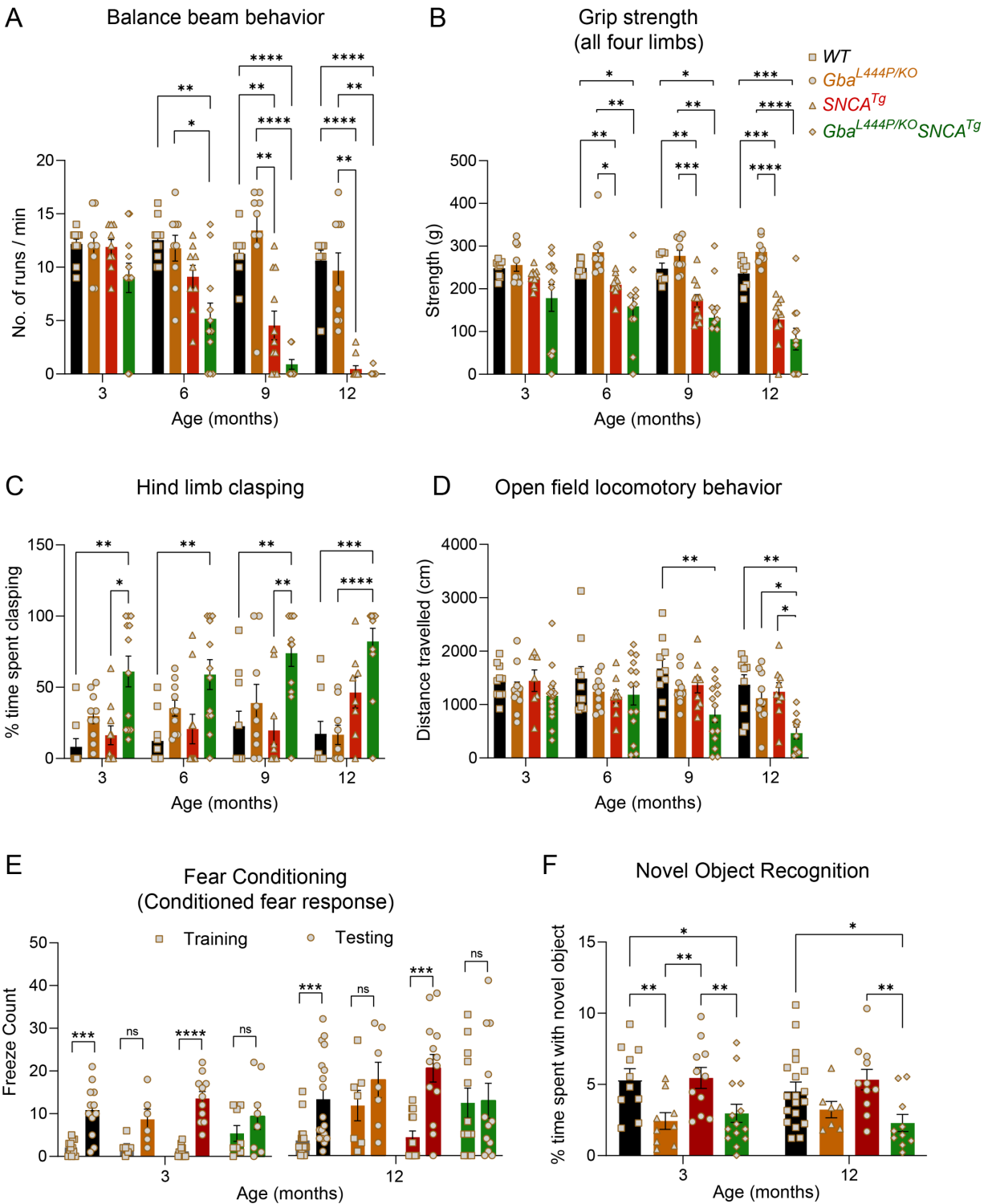
- 704 37. Dopeso-Reyes, I.G., *et al.* Glucocerebrosidase expression patterns in the non-human primate
705 brain. *Brain Struct Funct* **223**, 343-355 (2018).
- 706 38. Herrera Moro Chao, D., *et al.* Visualization of Active Glucocerebrosidase in Rodent Brain with
707 High Spatial Resolution following In Situ Labeling with Fluorescent Activity Based Probes.
708 *PLoS One* **10**, e0138107 (2015).
- 709 39. Boddupalli, C.S., *et al.* Neuroinflammation in neuronopathic Gaucher disease: Role of
710 microglia and NK cells, biomarkers, and response to substrate reduction therapy. *Elife* **11**
711 (2022).
- 712 40. Banks, S.M.L., *et al.* Hsc70 Ameliorates the Vesicle Recycling Defects Caused by Excess α -
713 Synuclein at Synapses. *eNeuro* **7** (2020).
- 714 41. Xu, J., *et al.* α -Synuclein Mutation Inhibits Endocytosis at Mammalian Central Nerve
715 Terminals. *J Neurosci* **36**, 4408-4414 (2016).
- 716 42. Binotti, B., *et al.* The GTPase Rab26 links synaptic vesicles to the autophagy pathway. *Elife*
717 **4**, e05597 (2015).
- 718 43. Goldman, J.G., *et al.* Cognitive impairment in Parkinson's disease: a report from a
719 multidisciplinary symposium on unmet needs and future directions to maintain cognitive
720 health. *NPJ Parkinsons Dis* **4**, 19 (2018).
- 721 44. Cheng, X., *et al.* Impaired pre-synaptic plasticity and visual responses in auxilin-knockout
722 mice. *iScience* **26**, 107842 (2023).
- 723 45. Balleine, B.W. Animal models of action control and cognitive dysfunction in Parkinson's
724 disease. *Prog. Brain Res.* **269**, 227-255 (2022).
- 725 46. Fan, Y., *et al.* Experimental Models of Cognitive Impairment for Use in Parkinson's Disease
726 Research: The Distance Between Reality and Ideal. *Front Aging Neurosci* **13**, 745438 (2021).
- 727 47. Decourt, M., Jiménez-Urbieto, H., Benoit-Marand, M. & Fernagut, P.O. Neuropsychiatric and
728 Cognitive Deficits in Parkinson's Disease and Their Modeling in Rodents. *Biomedicines* **9**
729 (2021).
- 730 48. Tayebi, N., *et al.* Glucocerebrosidase haploinsufficiency in A53T α -synuclein mice impacts
731 disease onset and course. *Mol. Genet. Metab.* **122**, 198-208 (2017).
- 732 49. Mahoney-Crane, C.L., *et al.* Neuronopathic GBA1L444P Mutation Accelerates
733 Glucosylsphingosine Levels and Formation of Hippocampal Alpha-Synuclein Inclusions. *J.*
734 *Neurosci.* **43**, 501-521 (2023).
- 735 50. Lado, W., *et al.* Synaptic and cognitive impairment associated with L444P heterozygous
736 glucocerebrosidase mutation. *Brain* (2024).
- 737 51. Altay, M.F., *et al.* Development and validation of an expanded antibody toolset that captures
738 alpha-synuclein pathological diversity in Lewy body diseases. *NPJ Parkinsons Dis* **9**, 161
739 (2023).
- 740 52. Anderson, J.P., *et al.* Phosphorylation of Ser-129 is the dominant pathological modification of
741 alpha-synuclein in familial and sporadic Lewy body disease. *J. Biol. Chem.* **281**, 29739-29752
742 (2006).
- 743 53. Walker, D.G., *et al.* Changes in properties of serine 129 phosphorylated α -synuclein with
744 progression of Lewy-type histopathology in human brains. *Exp. Neurol.* **240**, 190-204 (2013).
- 745 54. Kellie, J.F., *et al.* Quantitative measurement of intact alpha-synuclein proteoforms from post-
746 mortem control and Parkinson's disease brain tissue by intact protein mass spectrometry. *Sci*
747 *Rep* **4**, 5797 (2014).
- 748 55. Fayyad, M., *et al.* Investigating the presence of doubly phosphorylated α -synuclein at tyrosine
749 125 and serine 129 in idiopathic Lewy body diseases. *Brain Pathol* **30**, 831-843 (2020).
- 750 56. Halliday, G., Hely, M., Reid, W. & Morris, J. The progression of pathology in longitudinally
751 followed patients with Parkinson's disease. *Acta Neuropathol* **115**, 409-415 (2008).
- 752 57. Gómez-Tortosa, E., Irizarry, M.C., Gómez-Isla, T. & Hyman, B.T. Clinical and
753 neuropathological correlates of dementia with Lewy bodies. *Ann. N. Y. Acad. Sci.* **920**, 9-15
754 (2000).

- 755 58. Lashuel, H.A., *et al.* Revisiting the specificity and ability of phospho-S129 antibodies to
756 capture alpha-synuclein biochemical and pathological diversity. *NPJ Parkinsons Dis* **8**, 136
757 (2022).
- 758 59. Delic, V., *et al.* Sensitivity and specificity of phospho-Ser129 α -synuclein monoclonal
759 antibodies. *J. Comp. Neurol.* **526**, 1978-1990 (2018).
- 760 60. Furderer, M.L., *et al.* A Comparative Biochemical and Pathological Evaluation of Brain
761 Samples from Knock-In Murine Models of Gaucher Disease. *Int J Mol Sci* **25** (2024).
- 762 61. Pastores, G.M. Neuropathic Gaucher disease. *Wien Med Wochenschr* **160**, 605-608 (2010).
- 763 62. Imbalzano, G., *et al.* Neurological symptoms in adults with Gaucher disease: a systematic
764 review. *J Neurol* **271**, 3897-3907 (2024).
- 765 63. Sah, S., *et al.* Cortical synaptic vulnerabilities revealed in a α -synuclein aggregation model of
766 Parkinson's disease. *bioRxiv*, 2024.2006.2020.599774 (2024).
- 767 64. Terry, R.D., *et al.* Physical basis of cognitive alterations in Alzheimer's disease: synapse loss
768 is the major correlate of cognitive impairment. *Ann. Neurol.* **30**, 572-580 (1991).
- 769 65. Berezcki, E., *et al.* Synaptic proteins predict cognitive decline in Alzheimer's disease and Lewy
770 body dementia. *Alzheimers Dement* **12**, 1149-1158 (2016).
- 771 66. Berezcki, E., *et al.* Synaptic markers of cognitive decline in neurodegenerative diseases: a
772 proteomic approach. *Brain* **141**, 582-595 (2018).
- 773 67. Whitfield, D.R., *et al.* Assessment of ZnT3 and PSD95 protein levels in Lewy body dementias
774 and Alzheimer's disease: association with cognitive impairment. *Neurobiol Aging* **35**, 2836-
775 2844 (2014).
- 776 68. Vidyadhara, D.J., *et al.* Dopamine transporter and synaptic vesicle sorting defects initiate
777 auxilin-linked Parkinson's disease. *bioRxiv*, 2022.2002.2004.479203 (2022).
- 778 69. Nalls, M.A., *et al.* Identification of novel risk loci, causal insights, and heritable risk for
779 Parkinson's disease: a meta-analysis of genome-wide association studies. *Lancet Neurol* **18**,
780 1091-1102 (2019).
- 781 70. Leung, H.W., Foo, G. & VanDongen, A. Arc Regulates Transcription of Genes for Plasticity,
782 Excitability and Alzheimer's Disease. *Biomedicines* **10** (2022).
- 783 71. Vallortigara, J., *et al.* Dynamin1 concentration in the prefrontal cortex is associated with
784 cognitive impairment in Lewy body dementia. *F1000Res* **3**, 108 (2014).
- 785 72. Piromalli Girado, D., Miranda, M., Giachero, M., Weisstaub, N. & Bekinschtein, P. Endocytosis
786 is required for consolidation of pattern-separated memories in the perirhinal cortex. *Front Syst*
787 *Neurosci* **17**, 1043664 (2023).
- 788 73. Di Paolo, G., *et al.* Decreased synaptic vesicle recycling efficiency and cognitive deficits in
789 amphiphysin 1 knockout mice. *Neuron* **33**, 789-804 (2002).
- 790 74. Ito, Y., *et al.* Sphingolipids mediate polar sorting of PIN2 through phosphoinositide
791 consumption at the trans-Golgi network. *Nat Commun* **12**, 4267 (2021).
- 792 75. Capasso, S., *et al.* Sphingolipid metabolic flow controls phosphoinositide turnover at the trans-
793 Golgi network. *EMBO J.* **36**, 1736-1754 (2017).
- 794 76. Mistry, P.K., *et al.* Glucocerebrosidase gene-deficient mouse recapitulates Gaucher disease
795 displaying cellular and molecular dysregulation beyond the macrophage. *Proc Natl Acad Sci*
796 *U S A* **107**, 19473-19478 (2010).
- 797 77. Finak, G., *et al.* MAST: a flexible statistical framework for assessing transcriptional changes
798 and characterizing heterogeneity in single-cell RNA sequencing data. *Genome Biol* **16**, 278
799 (2015).
- 800 78. Yu, G., Wang, L.G., Han, Y. & He, Q.Y. clusterProfiler: an R package for comparing biological
801 themes among gene clusters. *Omics* **16**, 284-287 (2012).

802

803

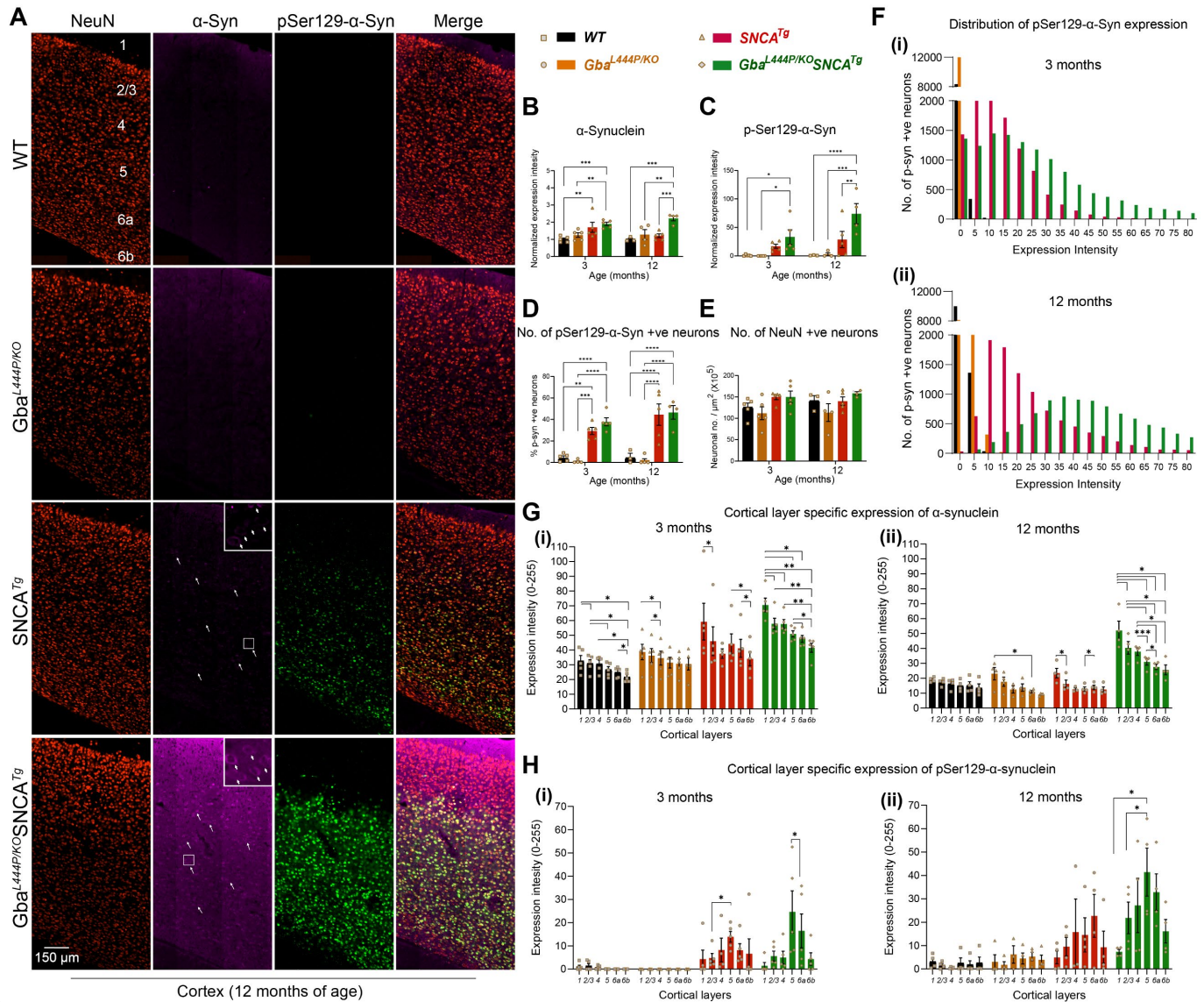
804 **Figures:**



805
 806 **Figure 1: *Gba* mutation worsens motor deficits in *SNCA* tg mice and independently leads**
 807 **to cognitive dysfunction.** WT, *Gba*, *SNCA* tg and *Gba*-*SNCA* mice cohorts were evaluated in
 808 four motor and two cognitive behavior tests in a longitudinal manner. **A.** Balance beam behavior.
 809 **B.** Grip strength of all four limbs. **C.** Hind limb claspings behavior. **D.** Open field locomotory

810 behavior. **E.** Fear conditioning test. **F.** Novel object recognition. $n = 9-12$ mice for motor behavior
 811 and 6-19 for cognitive behavior, both sexes were used. Data are presented as mean \pm SEM. ns -
 812 not significant; * $p < 0.05$, ** $p < 0.01$, *** $p < 0.001$, **** $p < 0.0001$

813



814

815 **Figure 2: Gba mutation exacerbates α -synuclein pathology in the cortices of SNCA tg mice.**

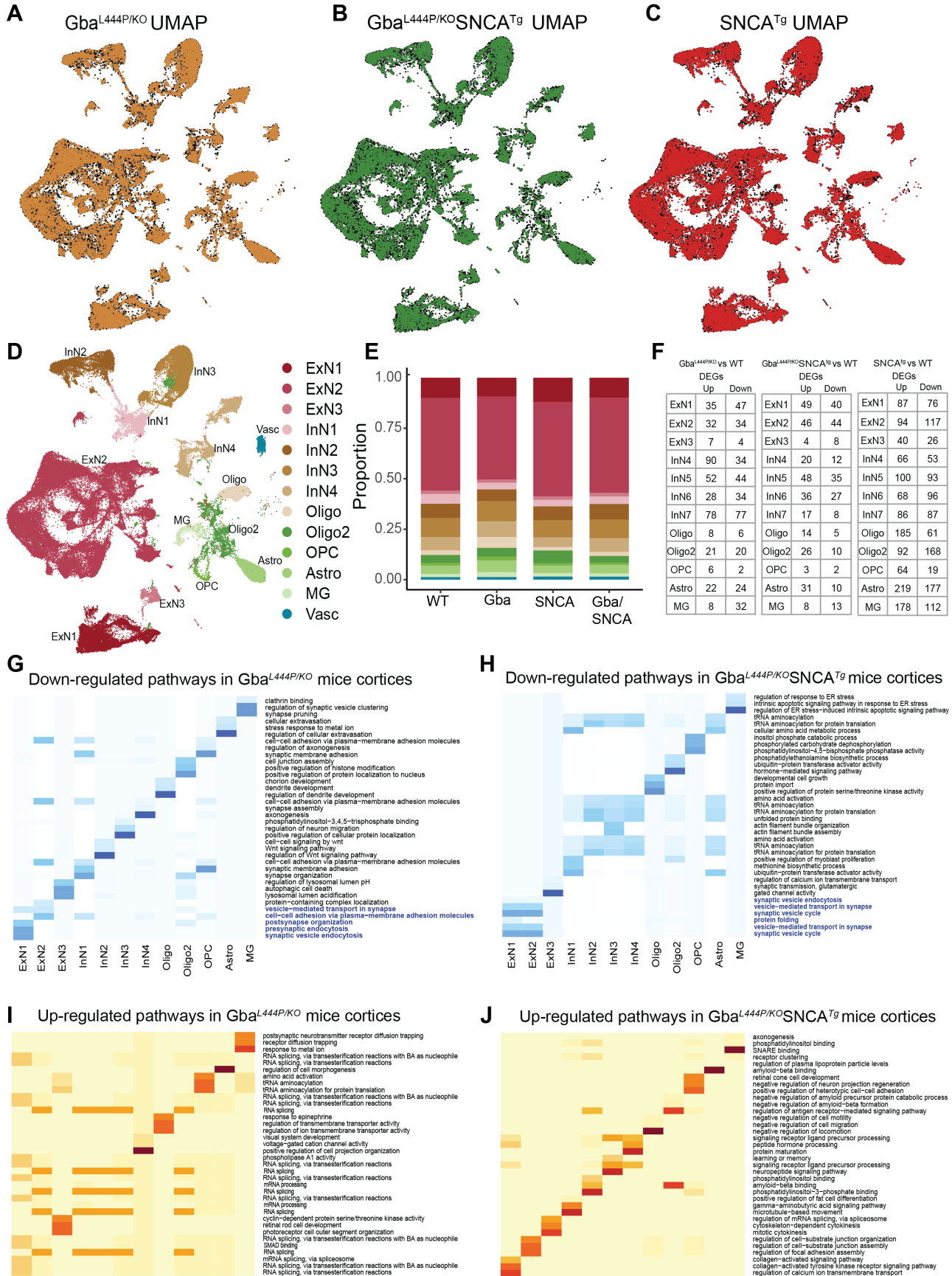
816 **A.** Representative images of cortices of WT, Gba, SNCA tg, and Gba-SNCA mice (12 months)
 817 immunostained for NeuN (red), α -synuclein (magenta) and pSer129- α -syn (green). Note
 818 increased α -synuclein levels along with redistribution to neuronal soma (arrow) and pSer129- α -
 819 syn expression in the Gba-SNCA double mutant when compared to SNCA tg mice. **B.** Cortical α -
 820 synuclein expression at 3 and 12 months, normalized to respective WT average at each time
 821 point. **C.** Cortical pSer129- α -syn expression at 3 and 12 months, normalized to respective WT
 822 average at each time point. **D.** Percentage of cortical neurons positive for pSer129- α -syn at 3 and
 823 12 months. **E.** NeuN positive cortical neuronal number at 3 and 12 months. **F.** Distribution of
 824 pSer129- α -syn expression intensity (Range of 0-255) in the cortical neurons at 3 months (i, WT:
 825 Mean = 0.35, 25% Percentile = 0.0024, 75% Percentile = 0.1252; Gba: Mean = 0.04, 25%

826 Percentile = 0, 75% Percentile = 0.0058; SNCA tg: Mean = 13.05, 25% Percentile = 5.211, 75%
827 Percentile = 18.534; Gba-SNCA: Mean = 23.781, 25% Percentile = 9.221, 75% Percentile =
828 33.972) and 12 months (ii), WT: Mean = 1.28, 25% Percentile = 0.439, 75% Percentile = 1.731;
829 Gba: Mean = 1.482, 25% Percentile = 0, 75% Percentile = 2.124; SNCA tg: Mean = 26.282, 25%
830 Percentile = 12.357, 75% Percentile = 32.834; Gba-SNCA: Mean = 53.741, 25% Percentile =
831 32.233, 75% Percentile = 66.691) of age. **G.** Cortical layer specific expression of α -synuclein at
832 3 (i) and 12 (ii) months of age. **H.** Cortical layer specific expression of pSer129 α -syn at 3 (i) and
833 12 (ii) months of age. n= 3-6, sex balanced. Data are presented as mean \pm SEM. ns - not
834 significant; *p < 0.05, **p < 0.01, ***p < 0.001, ****p < 0.0001. Scale = 150 μ m

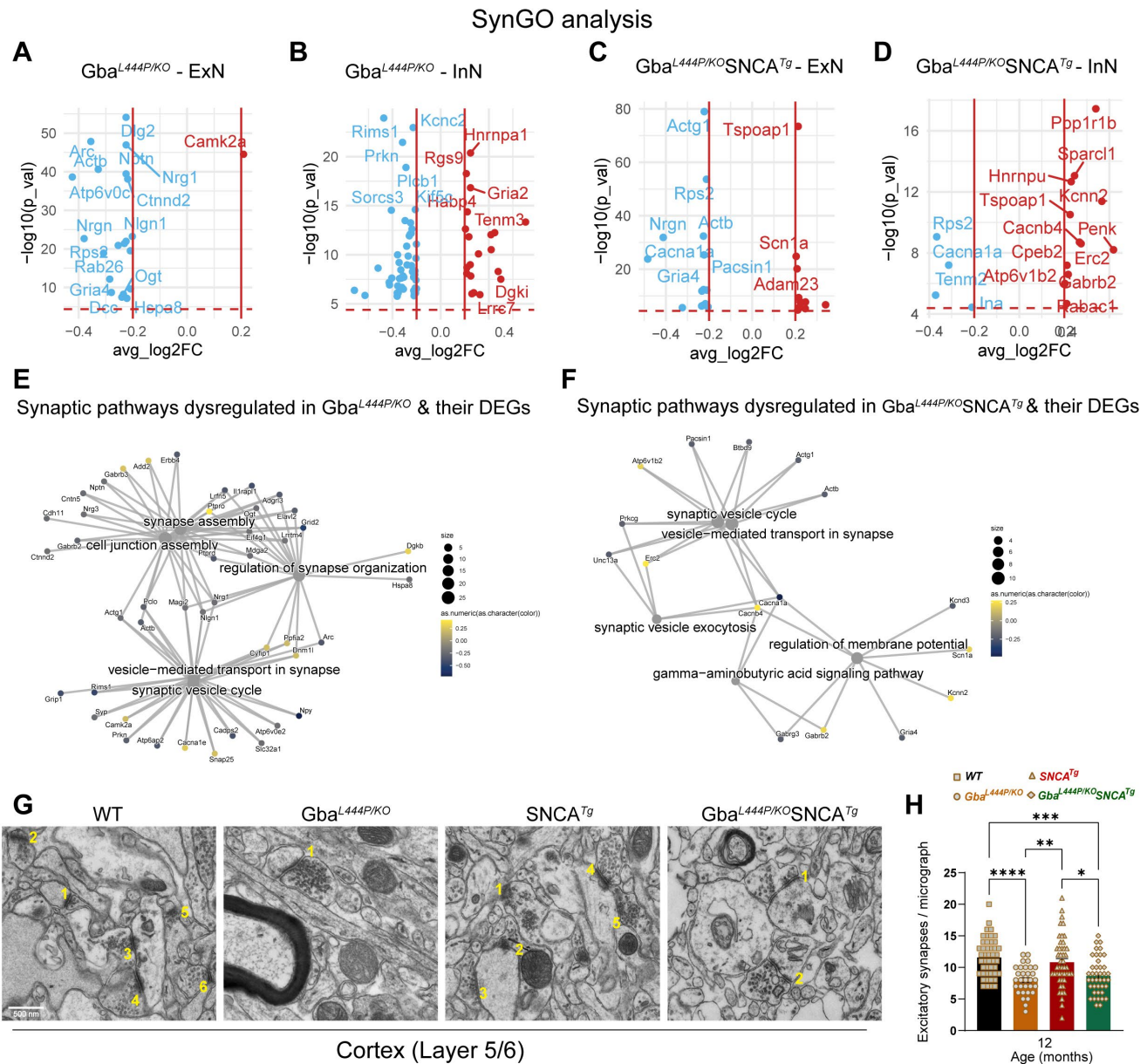
835

836

837

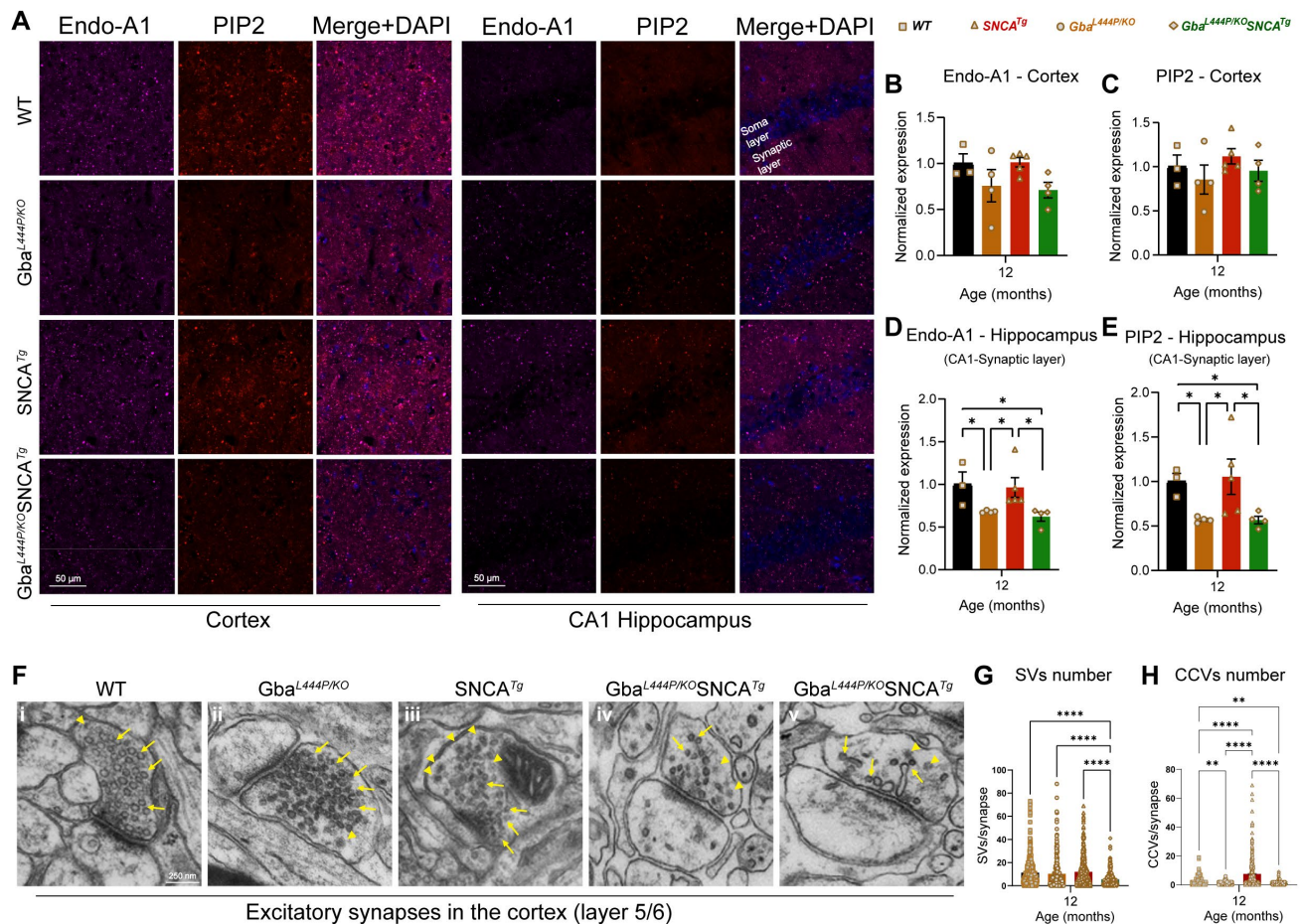


839 **Figure 3: Cell type distribution, differential gene expression, and cellular pathway changes**
 840 **in cortex.** Uniform Manifold Approximation and Projection (UMAP) dimension reduction for **A.**
 841 **Gba** (Amber), **B.** **Gba-SNCA** (Green) and **C.** **SNCA tg** (Red) overlaid over WT (Black) mouse
 842 cortical snRNAseq expression. **D.** UMAP showing clusters of cortical cell types identified by
 843 expression signatures. In **A-D**, UMAP 1 is shown on the x-axis and UMAP 2 on the y-axis. **E.**
 844 Proportions of the cell types in the cortices of wild type and transgenic mice. **F.** The number of
 845 differentially expressed genes (DEGs) per cell type in **Gba**, **Gba-SNCA**, and **SNCA** mutant mice
 846 after Bonferroni-correction for genome-wide comparisons and filtering out of genes with \log_2FC
 847 < 10.21 . **G-J.** Heatmap with the significantly down- and up-regulated gene ontology (GO) biological
 848 pathway alterations in 12 month old (**G, I**) **Gba**- and (**H, J**) **Gba-SNCA** mice, for each neuronal
 849 cluster type, revealed by unbiased analysis of enrichment of genome-wide corrected DEGs.
 850
 851



852

853 **Figure 4: Analysis of synapse related gene expression in *Gba* and *Gba*-SNCA neurons**
 854 **shows similar deficits in synapse vesicle cycling. A-D.** Analysis of significant DEGs that
 855 participate in synapse function, as annotated by SynGO, after Bonferroni-correction in excitatory
 856 (ExN1-3, **A, C**) and inhibitory (InN1-4, **B, D**) neurons. All genes with $\log_2FC < 0.2$ were filtered
 857 out. **E, F.** Cnet plots of differentially expressed synapse associated genes as annotated by
 858 SynGO, in **(E)** *Gba*⁻, and **(F)** *Gba*-SNCA mice cortices, after Bonferroni-correction for multiple
 859 comparisons. **G.** Electron micrographs of cortical layer 5/6 number for excitatory synapses. **H.**
 860 Quantitation of excitatory synapses in the cortical layer 5/6. Data are presented as mean \pm SEM,
 861 Scale = 500 nm, * $p < 0.05$, *** $p < 0.001$., N=2 brains in WT, SNCA tg, and *Gba*-SNCA mice, and 1
 862 brain in *Gba* mutant mice. 23-25 micrographs/genotype. 863



864 **Figure 5: Decreased expression of SVE markers and loss of SVs in *Gba* mutants. A.**
 865 Representative images showing cortical and CA1 hippocampal expression of endophilin-A1
 866 (Endo-A1) and phosphatidylinositol 4,5-bisphosphate (PIP2), two markers of synaptic vesicle
 867 endocytosis, in WT, *Gba*, SNCA tg, and *Gba*-SNCA mice at 12 months of age. **B.** Cortical Endo-
 870 A1 expression at 12 months, normalized to WT average. **C.** Cortical PIP2 expression at 12
 871 months, normalized to WT average. **D.** Endo-A1 expression in the CA1 Hippocampal synaptic
 872 layer, normalized to WT average. **E.** PIP2 expression in the CA1 hippocampal synaptic layer,
 873 normalized to WT average. Data are presented as mean \pm SEM. Scale = 50 μ m. * $p < 0.05$. n=4-5
 874 brains/genotype. **F.** Electron micrographs of excitatory synapses in cortical layer 5/6 showing
 875 synaptic vesicles (SVs, arrows) and clathrin-coated vesicles (CCVs, arrowheads) in WT (i), *Gba*
 876 mutant (ii), SNCA tg (iii), and *Gba*-SNCA (iv and v) mice. Note SVs with variable shapes and

877 sizes in Gba-SNCA synapse (**v**). **G-H**. Quantitation of SVs (**G**) and CCVs (**H**) in the excitatory
878 synapses of the cortical layer 5/6. Data are presented as mean \pm SEM, Scale = 250 nm, * $p < 0.05$,
879 ** $p < 0.01$, **** $p < 0.0001$, N=2 brains in WT, SNCA tg, and Gba-SNCA mice, and 1 brain in Gba
880 mutant mice. 23-25 micrographs, 150-300 synapses, per genotype.
881